Dynamics of cluster anions: a detailed look at condensed-phase interactions

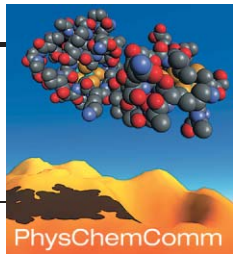

Perspective

Andrei Sanov*[a] and W. Carl Lineberger[b]

[a]*Department of Chemistry, University of Arizona, Tucson, Arizona 85721-0041, USA. E-mail: sanov@u.arizona.edu*
[b]*JILA and Department of Chemistry and Biochemistry, University of Colorado, Boulder, Colorado 80309-0440, USA. E-mail: wcl@jila.colorado.edu*

Received 20th September 2002, Accepted 5th November 2002
First published as an Advance Article on the web 19th November 2002

This Perspective reflects on several recent advances in the studies of structure and dynamics of cluster anions, bridging the gap between 'cluster' and condensed phases. Applications involving photofragment and photodetachment spectroscopy, as well as femtosecond time-resolved experiments, are described. Special emphasis is given to the effects of microscopic solvation on the electronic structure and reactivity of negative ions in heterogeneous and homogeneous cluster environments. Some recent breakthroughs in experimental methodology are also outlined, in particular the application of photofragment and photoelectron methods and the imaging technique to the studies of molecular cluster anions.

1. Introduction

Clusters have long fascinated chemists with the unique opportunities they offer for studies of intermolecular interactions implicated in practically all areas of chemistry, particularly in solvation. Ionic clusters are especially appealing for experimental studies of reactions, as in their well-defined microscopic environments the chemical dynamics can be examined at an unprecedented level of detail. Clusters are used as model micro-solutions that simplify the interpretation of solvation effects at a molecular level.[1–4] Such detailed analysis is difficult to achieve in macroscopic media, such as liquids, solids, or high-pressure gases, because of the poorly defined solvent coordination and the very large number of pairwise interactions involved. These characteristics of condensed environments usually require an averaged, *i.e.* statistical, rather than dynamical, description of bulk properties.

Despite their relatively small size, clusters retain many characteristics of the bulk media that make the condensed-phase dynamics as rich as they are. One central question in cluster studies is: how much matter is needed for physical laws associated with bulk materials to be applicable? The multitude of intermolecular interactions in clusters affords chemical reactions a variety of pathways and mechanisms that attracted the interest of many generations of chemists. The origin of the field of cluster chemistry can be traced back to the early studies of colloids, aerosols, and nucleation phenomena in the mid-nineteenth century, followed by an explosive growth during the twentieth century. For decades, many experimental and theoretical studies have been directed at deepening the understanding of detailed mechanisms of reactions within clusters. This paper is not intended to offer a comprehensive review of the vast field. Its scope is limited to recent photodissociation and photodetachment studies of cluster anions, giving a perspective of the dynamics of photoinduced reactions in cluster anions and the bridge between the 'cluster' and condensed phases. A broader outlook on the advances in cluster research during the later part of the twentieth century can be found, for example, in the review by Castleman and Bowen.[1]

In particular, we concentrate on several recent advances in the quest for better understanding of solvent-induced effects on the electronic structure and reaction dynamics. The most obvious effect of solvation is the limitation of physical space available to the solute, whose dynamics are constrained by physical barriers imposed by the presence of other bodies. In addition, the solvent acts as an energy bath, opening a pathway for internal relaxation of the solute. However, the most challenging aspect of solvation is the perturbation of the electronic structure of both the solute and the solvent.

We discuss the role of solvent-induced perturbations of the electronic structure in determining the outcomes of chemical reactions. These perturbations are particularly important in reactions involving non-adiabatic transitions. It is emphasized that the strong interactions implicated in ionic solvation often cannot be considered as merely a 'perturbation' in the perturbation-theory sense. If the strength of these interactions is comparable to the bonding in the solute or/and the solvent, chemical transformations are possible and the structure of the cluster core may differ greatly from the corresponding unsolvated species.

The cumulative ion–solvent interactions in ionic clusters can be easily comparable to chemical bonding, lending the solvent a major role in determining the reaction outcomes. For example, I_2^-, one of the most studied ionic chromophores,[5–24] has a bond dissociation energy of 1.01 eV, compared to a typical solvent binding energy of $\sim$0.2 eV per solvent molecule.[21,25] Clearly, the collective effect of the solvent on the electronic structure of I_2^- cannot be viewed as a minor perturbation even in moderate-size clusters. Therefore, although the term 'perturbation' is used widely in this Perspective, it is often assumed to imply a considerable effect rather than a minor modification of state potentials and their couplings.

Different types of solvent-driven reactions require various degrees of such perturbation. In many cases, the perturbation present within a cluster is rather large, although the reaction could proceed, in principle, even if it were minimal. One example is the solvent-induced recombination, or caging, of photofragments.[5,6,17,20–53] The fundamental appeal of this process lies in that it involves both the breaking and remaking of chemical bonds, both occurring under the influence of the solvent. The classic I_2^- caging reactions[5–7,21,45,46,49] evolve on potential energy surfaces correlating with the lower I_2^- dissociation limit yielding the neutral I fragment in the ground spin–orbit state. In this case, the $I(^2P_{3/2})$ + I^-

recombination proceeds *via* a mechanism[54–56] common for caging in both neutral and ionic, gas and condensed[39,57–59] phase systems. According to this mechanism, the fragment separation is halted by the solvent that absorbs the translational energy. The fragments then recombine following the conversion at large separation to the ground I_2^- electronic state. Subsequently, the recombined I_2^- undergoes vibrational relaxation as the energy is transferred to the solvent. Although the I_2^- electronic structure is greatly perturbed by the solvent,[60–62] only modest solvent-induced coupling between electronic states is actually *needed*, as the states in question are asymptotically degenerate. In the framework of this straightforward mechanism, the solvent effects are overwhelming in magnitude compared to the 'probe' used to monitor them (*i.e.*, the caging process). Therefore, it is not surprising that one finds the recombination dynamics not to be overly sensitive to the details of cluster structure.

It is possible, however, that a much larger degree of solvent-induced perturbation of the solute may be required for the reaction to be possible in principle. A new type of caging reaction was discovered recently,[22,24,63] in which the I_2^- chromophore is dissociated *via* the $I^*(^2P_{1/2}) + I^-(^1S)$ channel. In this case, a simple reversal of fragment trajectories cannot result in recombination, because the $I^*(^2P_{1/2}) + I^-(^1S)$ potentials are not bound. Nevertheless, caging on the ground electronic state of I_2^- is observed, which requires electronic quenching of $I^*(^2P_{1/2})$ to precede the recombination. This crucial transition involves an energy gap of nearly 1 eV and is known to be extremely slow when occurring *via* radiative or collisional energy transfer mechanisms. Not surprisingly, this type of caging was found to exhibit more sensitivity to the details of solvent-shell structure and dynamics.

Many laboratory tools are available today for the studies of ionic clusters. Among the most basic probes of cluster-ion structure and dynamics are mass-spectroscopy, photoelectron spectroscopy,[64,65] photofragment spectroscopy, and several relatively new ultrafast pump–probe techniques. The field made a jump towards better-controlled and more comprehensive experimental studies with the introduction in the 1980s of the pulsed cluster-ion techniques,[3] coupled with advances in tandem time-of-flight mass-spectroscopy. Lineberger-type pulsed ion sources, now prevalent in many laboratories around the world, allow the preparation and subsequent mass-selection of internally cool ionic clusters of known composition and often predictable structure. Using a combination of photoelectron and photofragment spectroscopic techniques, the reaction dynamics in cluster ions can be studied on the molecular level, bridging the gap between the properties of isolated molecules and chemistry and physics of condensed-phase environments.

The next revolutionary experimental tool introduced into the field in the late 1980s and early 1990s is the coupling of ultrafast pump–probe techniques with photoelectron spectroscopy and photofragment measurements. Whereas the experiments in the frequency (energy) domain help characterize the chemical and electronic structure of the cluster anions studied, the addition of the femtosecond pump–probe delay coordinate allows to study the reactions in real time, putting a truly dynamical emphasis on the experiments. The Lineberger group demonstrated the utility of ultrafast photofragment spectroscopy in the studies of cluster ion dynamics,[20,66] while Neumark *et al.* developed a time-resolved variant of negative-ion photoelectron spectroscopy (PES), know as femtosecond PES, which allows observation of reactions through the window of evolving photoelectron spectra.[46] These developments became possible with the advent of powerful and versatile femtosecond lasers. Other important trends in the field of cluster anion dynamics involve the move towards more detailed approaches to photoelectron and photofragment measurements, such as detecting several particles (*e.g.*, photoelectrons and photofragments) in coincidence,[67–73] infrared spectroscopic characterization of the cluster ion vibrational modes and structures,[74,75] the photoelectron imaging[76–78] approach to negative-ion PES.[79–83]

In this Perspective, we discuss several recent benchmark studies of cluster anion structure and dynamics. Section 2 describes the predicted structures of heterogeneous cluster anions $I_2^-(OCS)_n$ and $I_2^-(CO_2)_n$. Section 3 explores the caging dynamics in these clusters, with a special emphasis on the solvent-induced spin–orbit relaxation occurring on a remarkably fast timescale. Section 4 presents an outlook on the structure and photochemistry of homogeneous cluster anions, using $(OCS)_n^-$, $(CO_2)_n^-$, and others as benchmark systems. Section 5 gives a brief summary of the paper and outlines future directions.

2. Structures of heterogeneous cluster anions

The structure of the solvent shell about the ionic core of the cluster plays a determining role in its dynamics. To illustrate the basic principles involved in shell formation, we discuss the qualitative aspects of building up the first shell of OCS or CO_2 molecules around an I_2^- cluster core. The structures of $I_2^-(OCS)_n$ and $I_2^-(CO_2)_n$ have been examined using molecular dynamics and a model-Hamiltonian approach in a number of publications by the Parson group.[22,35,62,84,85] Their findings are in agreement with a number of experimental observations, some of which are highlighted in the following sections.

In the $I_2^-(OCS)_n$ cluster ions the binding of the solvent to the anionic core is dominated by charge–dipole interactions between I_2^- and OCS, whereas in $I_2^-(CO_2)_n$, in the absence of a permanent CO_2 dipole moment, the charge–quadrupole interaction takes center stage.[84,86,87] The solvent–solvent interactions also play important roles in both structure and dynamics. For example, the known fact that carbon dioxide forms dry ice implies strong interactions within the CO_2 solvent shell.

Since the charge in unsolvated I_2^- is equally divided between the two I-atoms, electrostatic considerations dictate that in stepwise solvation the first solvent molecule is expected to bind near the waist of I_2^-. Thus, in $I_2^-\cdot OCS$ the positively charged S-end of the solvent points toward the I_2^- center of mass. In larger $I_2^-(OCS)_n$ clusters, solvent–solvent interactions are added and the above solvent orientation motif is modified to accommodate these interactions as well.

The most revealing minimum-energy $I_2^-(OCS)_n$ structures, determined by the Parson group, are shown in Fig. 1.[22] The first five OCS molecules were found to arrange themselves around the waist of I_2^- with the sulfur atoms about 3.6 Å from the I_2^- center of mass. The solvent molecules are tilted at about 117°, rather than pointing directly outward, as best seen in Fig. 1(a). In $I_2^-(OCS)_5$, the five OCS molecules complete a ring around I_2^-. The next five molecules form a second ring around one end of the solute, then a single OCS molecule fills the axial site, ''capping'' that end of the cluster and completing the half-shell structure of $I_2^-(OCS)_{11}$ shown in Fig. 1(b). It is notable that $I_2^-(OCS)_{11}$ corresponds to a prominent ''magic number'' in the $I_2^-(OCS)_n$ cluster mass-spectrum, *i.e.*, the $n = 11$ peak clearly stands out in intensity compared to its neighbors.[22] This observation supports the particularly stable structure of this cluster predicted by the Parson model. The other side of the $I_2^-(OCS)_n$ cluster shell is filled in a similar fashion, completing the first solvation shell with 17 OCS molecules [see Fig. 1(c)].

In $I_2^-(CO_2)_n$, the charge–quadrupole interactions with the cluster core result in CO_2 molecules lying ''flat'' with respect to I_2^-. Parson and co-workers have shown that the CO_2 molecules tend to first pack together on one side of I_2^-, as shown in Fig. 2 for $I_2^-(CO_2)_5$,[36,62,84,88] rather than form a 'ring' [compare the structure of $I_2^-(CO_2)_5$ to $I_2^-(OCS)_5$ in

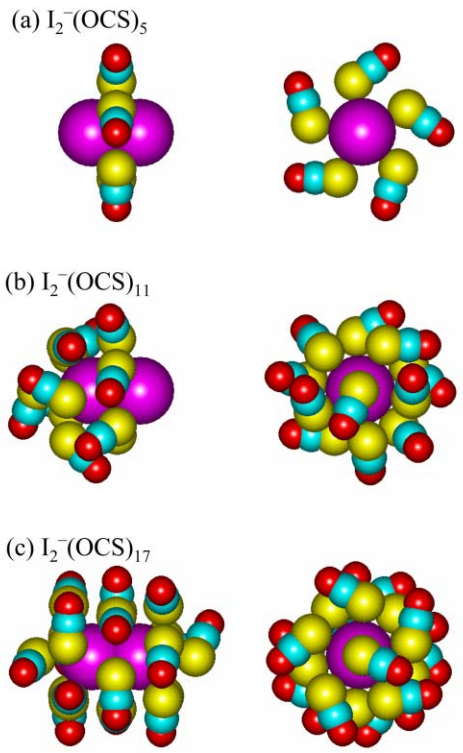

Fig. 1 Calculated minimum-energy structures of $I_2^-(OCS)_n$, $n = 5$, 11, and 17. Each structure is shown from two different angles, viewed perpendicular and along the I_2^- bond (left and right columns, respectively). These structures correspond to the isomers selected out of many nearly isoenergetic solvent configurations. While the general manner of solvent packing around I_2^- is reproduced in all low-energy isomers, local structural details, such as the relative orientation of neighboring OCS molecules, may vary. Adapted from ref. 22.

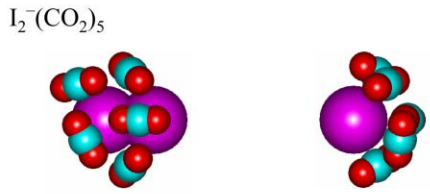

Fig. 2 Calculated minimum-energy structure of $I_2^-(CO_2)_5$ as viewed along the axes perpendicular (left) and parallel (right) to the I_2^- bond. Adapted from ref. 36.

Fig. 1(a)]. This type of packing maximizes the interactions within the CO_2 solvent shell itself. To the contrary, the ring structure of an OCS shell accentuates the strength of solvent–solute interactions, which are the strongest near the waist of the solute.

3. Photofragment caging dynamics in cluster ions

The photodissociation and recombination dynamics of I_2^- have been studied in both bulk liquids, such as water and alcohols (Barbara and co-workers),[5,6,45] and gas-phase clusters (Lineberger and Neumark groups).[20–25,48–50,53,66,89] Kondow and co-workers examined collisions of $I_2^-(CO_2)_n$ cluster ions with solid surfaces and observed a wedge-type splitting of the I_2^- bond by solvent CO_2 molecules upon cluster-surface collisions.[10,11,90,91] The dynamics of ionic clusters have been compared to the studies of I_2 recombination in solid rare-gas matrices by the Apkarian group.[39,57–59] Several groups provided extensive theoretical background for understanding the dissociation and recombination in clusters.[15,16,34,36,62,63,88,92] In particular, in the analysis of Parson and co-workers, the photofragmentation and caging are mediated by couplings of electronic states with differential charge character that is caused by interactions with the solvent.[36,47,62,88,93] It was shown that differential solvation of electronic states can lead to isoenergetic curve-crossing regions playing key roles in the relaxation and recombination dynamics.

We provide a perspective of the dynamics involved in caging by considering the photodissociation and recombination of I_2^- in clusters of the OCS[22–24,53] and CO_2[20,21,25,48,49,66,94–96] solvents. Together with the studies of I_2^- in N_2O[89] and Ar,[46,49,50,97] these experiments highlight the structural and dynamical effects of closed-shell solvents with different electrostatic properties.

The original studies[20,21,25,48,49] of I_2^- caging in clusters utilized the $A'\,^2\Pi_{g,1/2} \leftarrow X\,^2\Sigma^+_{u,1/2}$ transition centered near 790 nm to promote the dissociation of the chromophore. This transition, yielding the $I^- + I(^2P_{3/2})$ asymptotic products, is indicated by a red vertical arrow in Fig. 3, which shows the unperturbed I_2^- potentials calculated by Parson *et al.*[88] Later, striking new dynamics[22,24] were observed in the $I_2^-(OCS)_n$ and $I_2^-(CO_2)_n$ cluster ions excited at 395 nm *via* the $B\,^2\Sigma^+_{g,1/2} \leftarrow X\,^2\Sigma^+_{u,1/2}$ transition in the I_2^- chromophore (indicated by a blue vertical arrow in Fig. 4). This excitation accesses an electronic state correlating with the $I^- + I^*(^2P_{1/2})$ dissociation limit, where I^* indicates a spin–orbit-excited atomic fragment.

The dynamics observed at 790 and 395 nm are quite different. In a qualitative (and rather simplistic) description of the reaction following the near-IR excitation (Fig. 3), one might consider the solvent as playing a dual role. First, it acts as a physical barrier blocking the exit channel for

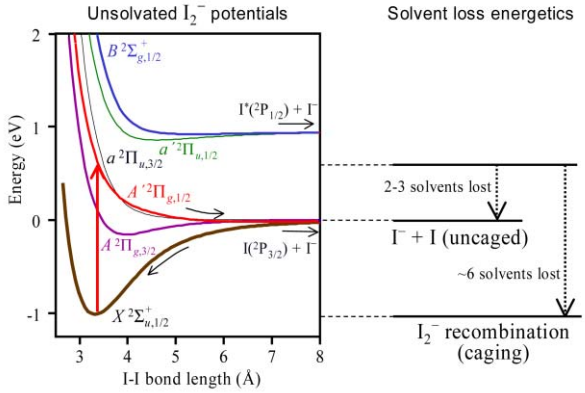

Fig. 3 Potential energy diagram of I_2^- (from ref. 88) and solvent loss energetics in 790 nm experiments on $I_2^-(OCS)_n$ or $I_2^-(CO_2)_n$.

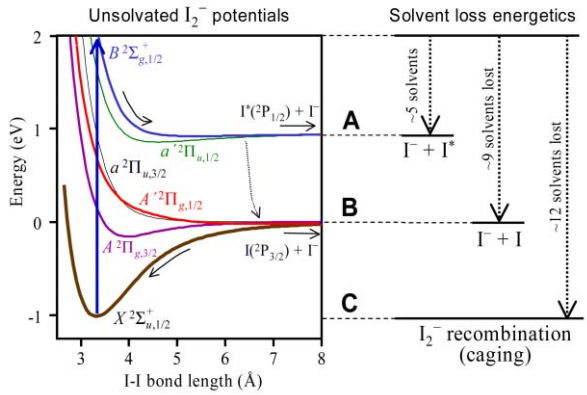

Fig. 4 Potential energy diagram of I_2^- (from ref. 88) and solvent loss energetics in 395 nm experiments on $I_2^-(OCS)_n$ or $I_2^-(CO_2)_n$.

photofragment escape from the cluster, thus triggering recombination. Second, it acts as an energy bath, enabling the relaxation of the caged chromophore and the cluster as a whole by evaporation of solvent molecules. The right-hand side of Fig. 3 illustrates the solvent loss energetics involved in the process. As each solvent molecule (OCS or CO_2) is bound to the cluster by $\sim$0.2–0.25 eV, the complete dissipation of the 790 nm photon energy requires the evaporation of $\sim$6 solvent molecules. Alternatively, if the I_2^- bond is not re-formed, only $\sim$2–3 solvent molecules are lost by the $I^-(OCS)_k$ fragments in the uncaged channel.

Although the true mechanism has been shown to be more complex,[36,62,84,92] this simplified picture does provide an initial understanding of the caging dynamics. This picture's seeming simplicity stems from the fact that it gives no significant account to the solvent-induced perturbation of I_2^- electronic structure. But at the same time, little perturbation is actually needed to envision the recombination process. The minimum perturbation required is that which would enable transitions from the bright state of I_2^- back to the ground electronic state, on which the recombination process ultimately terminates. Given that the A' state as well as two other excited states (A and a) are asymptotically degenerate with the X state, the required transitions can occur in the exit channel even with a minimum solvent-induced perturbation providing the state coupling. Thus, one obtains a tutorial (albeit somewhat misleading) picture of the reaction by considering the dissociation of largely unperturbed I_2^- confined inside the "solvent walls."

The situation is dramatically different at 395 nm (Fig. 4). The $B\ ^2\Sigma^+_{g,1/2} \leftarrow X\ ^2\Sigma^+_{u,1/2}$ transition in bare I_2^- leads to dissociation exclusively on the spin–orbit excited $I^- + I^*(^2P_{1/2})$ asymptote with a translational energy release of about 1.2 eV. No products are formed on the lower $I^- + I(^2P_{3/2})$ asymptote.[24] Thus, given the negligible probability of I^* quenching in collisions ($\sim 10^{-7}$–10^{-8} per collision),[98] the unperturbed electronic-state diagram in Fig. 4 predicts that practically no I_2^- caging is possible following the near-UV excitation.

The experiment, however, testifies to the contrary,[22,24] which raises the main question: Given the highly inefficient quenching of I^* in collisions, how do the dissociating $I^- + I^*(^2P_{1/2})$ fragments find their way to the lower spin–orbit asymptote, on which not only the recombination, but also the uncaged channel labeled B in Fig. 4 can evolve?

The quenching of spin–orbit excitation was found to be surprisingly efficient in the $I_2^-(OCS)_n$ and $I_2^-(CO_2)_n$ cluster ions. In general, three distinct pathways are observed (as labeled in Fig. 4): (A) the "uncaged" $I^-(OCS)_k$ products formed in coincidence with the excited $I^*(^2P_{1/2})$ fragments, which are ejected from the cluster; (B) the "uncaged" $I^-(OCS)_k$ products formed in coincidence with the quenched $I(^2P_{3/2})$ fragments; and (C) the "caged" $I_2^-(OCS)_k$ products.

The critical step in channels B and C is the quenching of the spin–orbit excitation. The competition between channels A–C is a delicate probe of the solvent-induced couplings between electronic states, which make the spin–orbit relaxation possible. In all three channels A–C, the excess energy is removed from the cluster by ejecting $(n - k)$ solvent molecules. Additionally, in channel A, almost 1 eV is carried away in the form of I^* spin–orbit excitation. As a result, the size distribution of the uncaged $I^-(OCS)_k$ products is in general bimodal, compared to a single-modal distribution of the caged $I_2^-(OCS)_k$ fragments.[22,24] The typical number of solvent molecules evaporated in each channel is indicated on the right-hand side of Fig. 4.

We continue our discussion of the dynamics in clusters by considering the cluster size-dependent caging probabilities. This is followed by the time-resolved dynamics of caging monitored in femtosecond pump–probe experiments.

Caging probabilities and their structural implications

First, consider the fraction of caged fragments observed in 790 nm dissociation of $I_2^-(OCS)_n$. This fraction, referred to as the caging probability, is plotted in Fig. 5 (open symbols) as a function of the number of solvent molecules.[22] No caged products are observed for clusters with $n < 3$, while for larger clusters the caging probability increases nearly monotonically with n, until a 100% caging is observed for $n \geqslant 17$. The theoretical simulations described in Section 2 predict that 17 OCS molecules comprise a complete solvent shell around I_2^- [Fig. 1(c)]. This is consistent with the experimental observation that $I_2^-(OCS)_{17}$ is the smallest cluster anion with the OCS solvent for which a 100% recombination of the chromophore is observed.

Despite the different nature of the dominant interactions in $I_2^-(OCS)_n$ and $I_2^-(CO_2)_n$, the 790 nm results for $I_2^-(CO_2)_n$, also shown in Fig. 5 (filled symbols),[49] are disappointingly similar to the findings for $I_2^-(OCS)_n$. Complete 790 nm caging in $I_2^-(CO_2)_n$ is observed for $n \geqslant 16$, consistent with the first solvent shell closing at n = 16–17, as predicted by the Monte-Carlo simulations.[62,84]

The monotonic increase in 790 nm caging probability and the lack of significant differences between the OCS and CO_2 solvents are consistent with the simplified picture of caging given in the introduction to this section. Even small perturbations of the I_2^- electronic structure would be sufficient to couple the asymptotically degenerate states, correlating to the lower dissociation limit. Therefore, the intricate details of the solvent–solute and solvent–solvent interactions are not too important. The main role of the solvent in this case indeed appears to be that of a physical obstacle in the exit channel of I_2^- dissociation and an energy bath. In this light, increasing the number of solvents bound to the chromophore naturally results in a monotonic increase in the caging probability.

Now consider the entirely different dynamics observed in the 395 nm experiment. The corresponding fraction of caged fragments is plotted in Fig. 6(a) for both $I_2^-(OCS)_n$ and $I_2^-(CO_2)_n$ cluster anions. As expected, the onset of 395 nm caging is observed in larger clusters, compared to 790 nm. However, the caging probability itself is no longer the only parameter characterizing the channel competition. From a dynamical viewpoint, perhaps of even greater interest is the probability of spin–orbit relaxation induced by the solvent. Regarding the diagram in Fig. 4, the spin–orbit relaxation is prerequisite for channels B and C. Therefore, the probability of quenching is given by adding together the respective branching ratios for the spin–orbit relaxed uncaged channel (B) and the

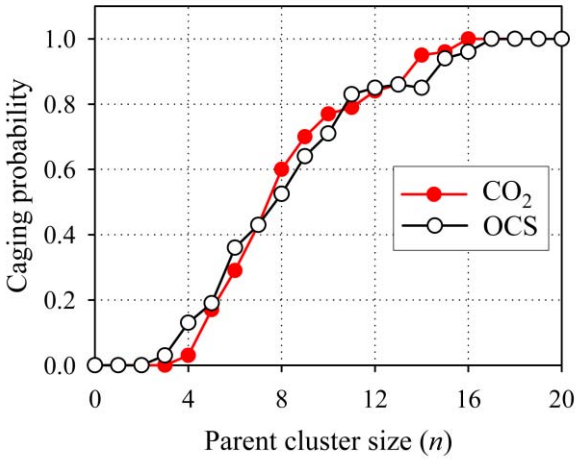

Fig. 5 Probabilities of recombination (caging) of the I_2^- chromophore in $I_2^-(CO_2)_n$ and $I_2^-(OCS)_n$ clusters following photoexcitation at 790 nm, as functions of the parent cluster size. Data from ref. 22 and 24.

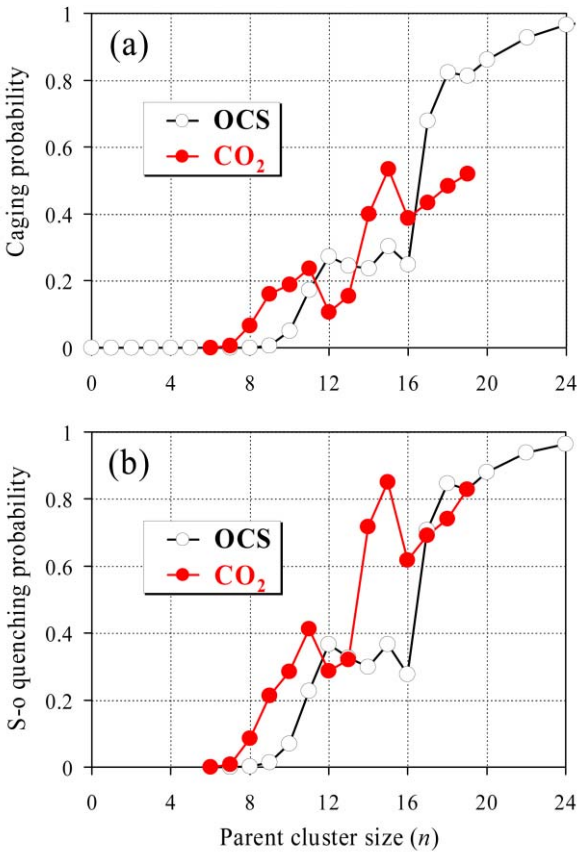

Fig. 6 (a) Probabilities of recombination (caging) of the I_2^- chromophore in $I_2^-(CO_2)_n$ and $I_2^-(OCS)_n$ clusters following photoexcitation at 395 nm, as functions of the parent cluster size. (b) Similar curves for the probability of I^* spin–orbit quenching. Data from ref. 22 and 24.

caged channel (C). The thus obtained spin–orbit quenching probability is plotted in Fig. 6(b) for both $I_2^-(OCS)_n$ and $I_2^-(CO_2)_n$ as a function of n.

The complete caging is not achieved for any of the parent clusters studied (*e.g.*, up to 26 solvent OCS molecules, for which the caging probability is 0.98). Still, recombination is the dominant reaction pathway for parent clusters with $n \geqslant 17$. What sets the 395 nm caging probability curves [Fig. 6(a)] aside from the corresponding 790 nm curves (Fig. 5) is their structured nature.

The 395 nm caging curve for the CO_2 solvent is not monotonic in the range of $n = 11$–16, while the corresponding curve for the $I_2^-(OCS)_n$ cluster ions exhibits a plateau in the same approximate range ($n = 12$–16), followed by a step-like nearly three-fold increase at $n = 17$. Notably, $n = 17$ is the smallest $I_2^-(OCS)_n$ cluster size for which 100% caging is observed at 790 nm and it corresponds to a cluster with a predicted complete solvent shell.

The sharp increase in caging upon addition of the 17th OCS molecule was attributed to a steric effect: the 17th molecule occupies the only remaining open site at the end of I_2^- [see Fig. 1(c)]. The occupation of this site closes the last collision-free escape route for $I_2^- \rightarrow I^- + I$ dissociation. The presence of solvent on the I_2^- dissociation coordinate also increases the likelihood of non-adiabatic quenching of I^*, which is prerequisite for recombination.

Another prominent feature of the $I_2^-(OCS)_n$ caging and spin–orbit quenching probability curves in Fig. 6 is the plateau at $n = 12$–16. No such plateau was observed for $I_2^-(CO_2)_n$, for which both caging and quenching in the same cluster size range exhibit seemingly erratic behaviors. It is revealing that the $I_2^-(OCS)_n$ plateau consists of exactly *five* cluster sizes, reminiscent of the theoretical prediction that the first OCS solvent shell around I_2^- consists of three *five*-membered OCS rings plus two end molecules "capping" the cluster (Fig. 1). The plateau thus corresponds to the formation of the third solvent ring around the chromophore. The lack of a similar plateau for $I_2^-(CO_2)_n$ is consistent with the qualitatively different structural motif of $I_2^-(CO_2)_n$, which is not based on solvent rings (see Fig. 2).

The suggested mechanism of the spin–orbit quenching and recombination is discussed following the examination of the timescales on which these processes transpire.

Time-resolved dynamics of caging

The application of time-resolved techniques to chemical processes occurring on a femtosecond time scale has been one of the most important developments in reaction dynamics during the past decade.[46,77,99–105] In particular, the application of femtosecond pump–probe spectroscopy to cluster anions allowed examination of the relaxation and energy-transfer processes at unprecedented levels of detail.

The dissociation of the I_2^- chromophore within a cluster destroys the cluster's ability to absorb visible/near-IR light, resulting in transient bleaching, while the ensuing recombination revives the absorption cross-section. A second photon can probe either the $A'\ ^2\Pi_{g,1/2} \leftarrow X\ ^2\Sigma^+_{u,1/2}$ or the $a\ ^2\Pi_{u,3/2} \leftarrow A\ ^2\Pi_{g,3/2}$ transition.[21] The transient bleaching and absorption recovery thus provide a way for examination of real-time dynamics of caging by monitoring the delay-dependent yield of two-photon products in a pump–probe experiment. Such measurements using a 720–790 nm pump and probe were performed (among others)[21,49,89] on $I_2^-(CO_2)_n$ and $I_2^-(OCS)_n$ cluster ions.[21,23,24,49,53] The experiments revealed picosecond time-scales of the recombination and subsequent relaxation.

For example, Fig. 7(a) shows the absorption recovery curves for $I_2^-(OCS)_7$ and $I_2^-(OCS)_{17}$ obtained in 790 nm pump–probe experiments. In this case, the positive and negative delays correspond to the reversal of the order of the identical pump and probe photons and therefore convey the same dynamical information. The near disappearance of signal at a zero delay reflects the bleaching of the probe absorption due to the dissociation of the chromophore by the pump photon. The fast ($\sim$2 ps) rise is absorption recovery observed following 790 nm excitation of $I_2^-(OCS)_{17}$ is attributed to the initial recombination of the $I(^2P_{3/2})$ and I^- fragments. In this delay range, the probe photon is absorbed by I_2^- in one of the excited electronic states or a highly excited vibrational level of the ground state.[48,92] The 2 ps timescale corresponds to the period of the pseudo-vibrational $I\cdot\cdot I^-$ motion in the system excited above its dissociation threshold but constrained by the solvent. The bump appearing in the $I_2^-(OCS)_{17}$ absorption recovery curve at 2 ps is characteristic of the coherent $I\cdot\cdot I^-$ motion[23,48] within the cluster. In $I_2^-(OCS)_7$ the solvent cage is smaller, the dynamics are correspondingly slower and not so much coherent, and the 2 ps peak does not appear. The longer timescale dynamics in both $I_2^-(OCS)_7$ and $I_2^-(OCS)_{17}$, characterized by the pump–probe signal leveling off after $\sim$20 ps, reflect the internal relaxation of the caged chromophore.

An alternative perspective of these dynamics is provided by time-resolved photoelectron spectroscopy. While the photofragment measurements, by their very definition, focus primarily on the nuclear degrees of freedom, Neumark and co-workers pioneered an experimental approach that shifts the emphasis to the evolving electronic structure.[46] Femtosecond photoelectron spectroscopy of cluster anions is used to probe the transient states and changing environment of the chromophore or its fragments by recording transient spectra of the electrons detached from the excited cluster with a delayed UV probe pulse.

When these measurements are carried out on the isolated

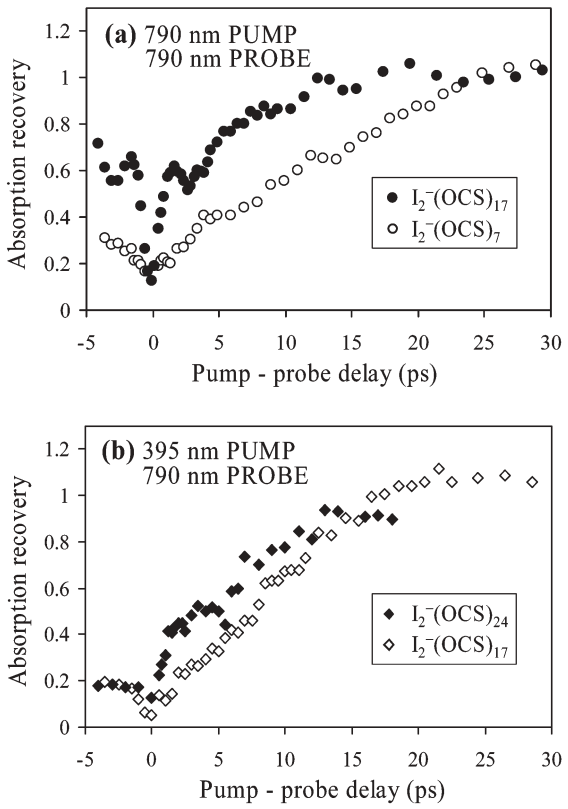

Fig. 7 Delay-dependent absorption recoveries of indicated $I_2^-(OCS)_n$ cluster ions following the excitation at (a) 790 nm and (b) 395 nm. In (b), the relaxation processes leading to I_2^- caging include the spin–orbit relaxation of I^*, while in (b) the spin–orbit relaxation step is not involved. Adapted from ref. 24.

chromophore, the time-dependent photoelectron spectra reflect the timescale of the dissociation process.[17–19] In the experiments on I_2^- embedded in Ar or CO_2 clusters,[46,94,97] the transient spectra reveal that after the charge localizes on one of the chromophore fragments, the photoelectron bands exhibit a varying energetic shift due to interactions with the solvent. In small (*e.g.*, $n = 6$) Ar clusters, this shift persists for $\sim$1 ps, which is the time required for I^- to escape from the cluster.[46] Parson group's molecular dynamics calculations that model the solvent interactions with the localizing charge predicted shifts in electron affinity of the cluster that agree well with Neumark's measurements.[47,93] In larger clusters, the transient photoelectron spectra reveal the recombination of I_2^- in both ground and excited electronic states, followed by vibrational relaxation and solvent evaporation.[94,97] The timescale of these processes are consistent with the timescales of caging observed by Lineberger and co-workers.[25,49]

To summarize, the fast rise in the $I_2^-(OCS)_{17}$ absorption recovery signal seen in Fig. 7(a) during the first couple of picoseconds reflects the timescale for I_2^- recombination on the lower spin–orbit asymptote. This approximate timescale is typical of I_2^- recombination in several molecular solvents (CO_2, N_2O, OCS). It is concluded that it takes $\sim$2 ps for the solvent shell to reverse the $I^- + I$ dissociation trajectories and direct the fragments towards recombination.

Similar photofragment measurements carried out with a 395 nm pump examined the dynamics on the upper spin–orbit asymptote of dissociating I_2^-. The qualitative zeroth-order picture of this process is illustrated in Fig. 4. The recovery curves for $I_2^-(OCS)_{17}$ and $I_2^-(OCS)_{24}$ in Fig. 7(b) reflect the cumulative timescales of spin–orbit relaxation and recombination. For $I_2^-(OCS)_{24}$, the initial rise in absorption recovery occurs on a timescale of $\sim$2 ps, similar to the period of solvent-induced coherent $I{\cdot\cdot}I^-$ motion observed following 720 or 790 nm excitation.[21,23,24,48,49] In the smaller $I_2^-(OCS)_{17}$ cluster, the recovery is slower, similar to the 720–790 nm results for smaller clusters.

To emphasize this analogy, compare the absorption recovery curves in Figs. 7(a) and (b). The cluster sizes in (a) and (b) are purposefully different, as they were selected for the similarity of the respective timescales. (Qualitatively, adding extra solvent molecules counter balances the effect of doubling the energy pumped into the cluster at 395 nm, compared to 790 nm.) Despite the differences in detail, the timescales of caging following 395 and 790 nm excitations are very similar, indicating that the spin–orbit relaxation step implicated in Fig. 7(b), but not in Fig. 7(a), must be fast on the overall timescale of the reaction.

Solvent-mediated charge transfer as a fast spin–orbit quenching mechanism

The detailed analysis of 395 nm caging dynamics by the Lineberger and Parson groups shows[22,24,63] that the quenching of spin–orbit excitation, followed by I_2^- recombination, is only possible because of the strong perturbation of the I_2^- electronic structure by the solvent. Other mechanisms, failing to consider explicitly the perturbed I_2^- potentials (*e.g.*, radiative decay or collisional quenching), have been ruled out based on experimental and theoretical evidence.[24] Here, we outline the solvent-asymmetry mediated electron transfer model, first suggested by Maslen *et al.*[60] and developed by Delaney *et al.*,[63] that has been accepted as an accurate view of the reaction.

The drawback of the collisional mechanism of I^* quenching is that it considers the I^- fragment as a mere spectator. This strategy fails in the cluster ion environment. As another clue calling for a different interpretation, I^* quenching on a picosecond timescale has not been observed in neutral environments. Thus, the proximity of I^- and the perturbed electronic structure of the $I^-\cdots I^*$ system are key to understanding the relaxation mechanism.

The energy gap between the two spin–orbit asymptotes in Fig. 4 can be bridged by the effects of solvation. Because of the substantial binding energy of OCS and CO_2 to a negatively charged cluster ($\sim$0.2 eV per molecule),[21,22,25] the relative electronic state energies are greatly affected by state-specific charge distributions and solvent asymmetry. In the example in the top portion of Fig. 8, the $I^- + I(^2P_{3/2})$ and $I^- + I^*(^2P_{1/2})$ electronic states are separated by 0.93 eV in the unsolvated $I{\cdot\cdot}I^-$ system (Fig. 8, top left). These states are degenerate with respect to switching the fragment positions (*i.e.*, $I^- + I$ *versus* $I + I^-$, and $I^- + I^*$ *versus* $I^* + I^-$). In the cluster environment, this degeneracy is lifted by asymmetric solvation of the fragment pair (Fig. 8, top right). If the charge is localized at the more solvated end of the cluster (*e.g.*, $X{\cdot}I^-{\cdot\cdot}I$, where X denotes the collective solvent), the corresponding state energy is lowered significantly. On the other hand, if the charge is localized on the least solvated end (*e.g.*, $X{\cdot}I{\cdot\cdot}I^-$), the solvation effect is less significant. If the energetic difference between the two charge/solvent configurations, termed the differential solvation energy ($\Delta\Phi$), is close to 0.93 eV, the $X{\cdot}I^-{\cdot\cdot}I^*$ and $X{\cdot}I{\cdot\cdot}I^-$ states may come into resonance, and a fast spin–orbit quenching transition becomes possible by an electron hoping from I^- to I^*.

Parson and co-workers developed this picture and identified the electronic states of I_2^- of different charge-switching character.[60-62] Their behavior under differential solvation is illustrated qualitatively in Fig. 8 (bottom). In the states with "normal" charge-switching character, the charge gravitates towards the more solvated end of I_2^-. Compared to unsolvated I_2^-, the energies of these states decrease with increasing $I{-}I^-$ separation due to more efficient solvation as the charge becomes more localized. To the contrary, the "anomalous" charge-switching states exhibit a charge distribution favoring

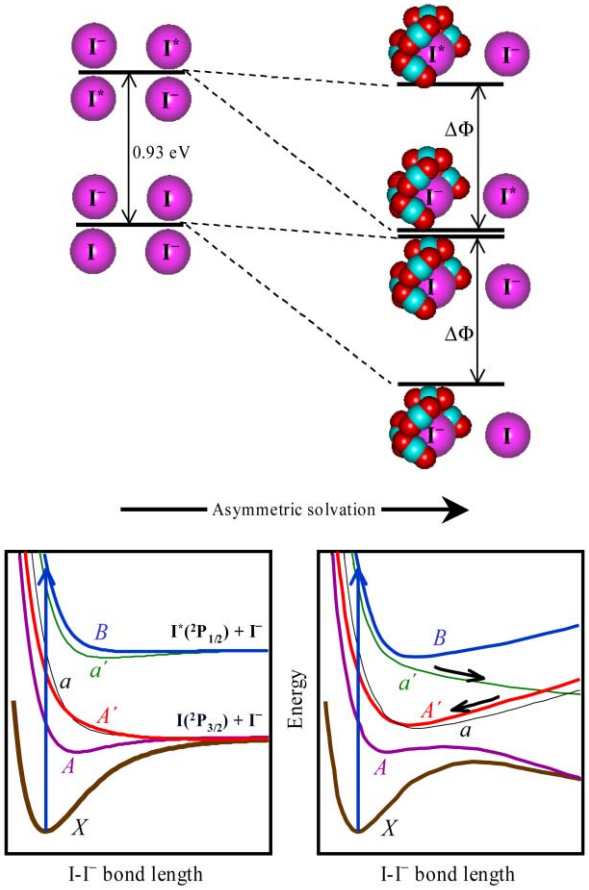

Fig. 8 Top: A qualitative energy diagram illustrating the mechanism of spin–orbit relaxation by solvent-mediated electron transfer from I^- to I^* in an asymmetrically solvated cluster. The required resonance of the $X{\cdot}I^-{\cdot\cdot}I^*$ and $X{\cdot}I{\cdot\cdot}I^-$ electronic states occurs when the differential solvation energy ($\Delta\Phi$) is equal to the spin–orbit energy gap in the I atom (0.93 eV). Adapted from ref. 24. Bottom left: A qualitative I_2^- potential energy diagram (unsolvated anion). Bottom right: A qualitative illustration of the behavior of "normal" and "anomalous" charge-switching states of I_2^- under the conditions of asymmetric solvation. The curve-crossings promote the $X{\cdot}I^-{\cdot\cdot}I^* \rightarrow X{\cdot}I{\cdot\cdot}I^-$ electron-transfer transitions, quenching the spin–orbit excitation of the I fragment.

the least solvated end of the chromophore. The energy of these states increases in dissociation, as the I^-–solvent interaction drops with increasing I–I^- distance. The resulting curve-crossings, implicated in Fig. 8 (bottom right), make a $X{\cdot}I^-{\cdot\cdot}I^* \rightarrow X{\cdot}I{\cdot\cdot}I^-$ transition possible. Following that, the electrostatic attraction between the solvent and I^- will tend to reverse the dissociation trajectory towards I_2^- recombination.

Fig. 8 is only a qualitative illustration, oversimplifying the energetics and dynamics of quenching. The number and configuration of solvent molecules in the figure are chosen arbitrarily to satisfy the $\Delta\Phi \approx 0.93$ eV requirement. In reality, transient resonances between different electron-transfer states are possible starting from a wide range of initial solvent configurations, including nearly symmetric ones. As the cluster breaks up and the charge localizes on one of the fragments, the initial symmetry, if any, is always destroyed and as long as the number of solvent molecules in the cluster is sufficient, the required curve crossing is possible at some cluster geometry.

The dynamics on the ground spin–orbit asymptote following the spin–orbit relaxation are reflected in the relative yields of channels B and C (defined in Fig. 4). In the 790 nm experiment, *all* dynamics transpire on this asymptote, and in small clusters the dissociation is naturally favored over the recombination.[22,25,49,89] To the contrary, at 395 nm no preference is observed for $I^- + I(^2P_{3/2})$ dissociation over the recombination, even in the smallest clusters in which the spin–orbit quenching is possible. Evidently, this is due to the restrictions imposed by the spin–orbit relaxation step. The quenching can occur only if the number of solvent molecules in the cluster is sufficiently large, which by itself favors recombination. Additionally, following the electron transfer, the charge in the $X{\cdot}I{\cdot\cdot}I^-$ state localizes on the escaping fragment, which experiences a backward pull from the solvent. Thus, the solvent configurations that are prerequisite for quenching also favor recombination.

It is noteworthy that if electron transfer fails during the initial fragment separation on the $X{\cdot}I^-{\cdot\cdot}I^*$ state, the electrostatic force acting on the neutral fragment is weak, and the ensuing dynamics will favor cage escape. Consequently, the dynamical window for spin–orbit quenching is limited to the initial fragment separation, consistent with the fast timescale of caging observed experimentally. Since the quenching step does not add extra time to that needed for fragment separation and subsequent recombination, the similar caging timescales are to be expected at both 395 and 790 nm. This prediction is in accord with the remarkably similar behaviors reflected in Fig. 7(a) and (b).

The resonance condition for spin–orbit quenching by the solvent asymmetry mediated electron transfer is very sensitive to instantaneous solvent configurations.[63] Therefore, the caging reaction involving the spin–orbit relaxation is a sensitive probe of solvation, with the cluster structure playing an important role in the dynamics. In both $I_2^-(OCS)_n$ and $I_2^-(CO_2)_n$, the quenching and caging probabilities are rather smooth and monotonic outside the range of $n = 11$–17 (see Fig. 6). Only in this mid-size range, where the second half of the first solvent shell is believed to be constructed (*e.g.*, see Fig. 1), the curves deviate from the expected monotonic rise, such as the 790 nm trend seen in Fig. 5. For smaller clusters, the too few available solvent molecules restrict the quenching trajectories because of a limited number of extremely asymmetric solvent configurations that satisfy the requirement $\Delta\Phi \approx 0.93$ eV. Each additional solvent molecule loosens this constraint, boosting the quenching and caging probabilities. In the mid-size range ($n = 11$–17), the sufficient degree of differential solvation is achieved without imposing severe dynamical restrictions. In this size range, the details of cluster structure, not the mere number of solvent molecules, become crucial in determining the reaction outcomes. This trend continues until the first solvent shell is filled at $n = 16$–17. From there on, additional solvent molecules do not introduce significant energetic or structural changes, and the dynamics revert to a monotonic increase in caging probability with n.

4. Structure and photochemistry of homogeneous cluster anions

Some cluster anions, particularly the homogeneous clusters X_n^-, where X = CO_2, OCS, CS_2, H_2O, and others, pose additional questions concerning their structure that have to do with the chemical identity of the cluster core. The properties of the core are fundamental to the reactivity and dynamics. The first question that must be addressed is often whether the excess electron in the cluster anion is localized on a single monomer or shared between two (or more) monomer moieties.[1,106–115] In the limit of electron solvation,[116,117] the excess electron wave function is delocalized to such extent that the concept of a cluster core is no longer applicable.

These questions did not arise in the preceding discussion of solvated I_2^-. It was assumed implicitly that during the entire course of the reaction the charge stays localized on the chromophore or one of its fragments. This assumption is justified, to a degree, in heterogeneous cluster anions, such as $I_2^-{\cdot}X_n$, when there is a significant difference in the electron affinities (EA) between the species composing the cluster. Even

so, the electronic wave functions of negative ions tend to be diffuse, allowing for substantial overlap with the surrounding solvent. For example, even in such a small heterogeneous cluster anion as $I^-\cdot CO_2$, Neumark and co-workers observed a 175° bending of CO_2, attributed to a small amount of charge transfer from the I^- to the CO_2.[118–120] The experiments by Johnson and co-workers on hydrated cluster anions indicate the profound effect that the charge density has on the structure adopted by a water network bound to an ion.[121–126] Charge delocalization can be more important in larger clusters. In addition, charge-transfer-to-solvent excited states are available in both bulk solutions[116,127] and clusters.[128–133]

In the homogeneous water cluster anions $(H_2O)_n^-$, $n \geqslant 2$, the neutral solvent network deforms to trap a diffuse excess electron, forming microscopic precursors of the hydrated electron. Water cluster anions have long served as a favorite system for the studies of electron solvation and the transition between gas-phase (or cluster) and bulk properties.[134] The variety of interaction available in these cluster ions, including, but not limited to, hydrogen bonding and delocalized charge–dipole interactions, leads to interesting structure variations.[74,75,134,135] Significant molecular rearrangements upon electron attachment to a neutral cluster have been implicated in the formation of different structural isomers.[134]

Different puzzles pertaining to charge localization and structures are presented by cluster anions of CO_2, OCS, and CS_2. Since the mid-1980s, photofragment and photoelectron spectroscopies, as well as theoretical studies of $(CO_2)_n^-$, posed questions of size-dependent alternation between cluster structures adopting either the monomer or dimer anion cores.[107,108,112,136] Photoelectron spectroscopy revealed sharp discontinuities in the *n*-dependence of the vertical detachment energy of $(CO_2)_n^-$ cluster anions between $n = 6$ and 7 and between $n = 13$ and 14.[107,108] These discontinuities have been attributed to "core switching": a transformation of the charged cluster core from a delocalized-charge covalent $(CO_2)_2^-$ structure for $n < 6$ to CO_2^- for $7 \leqslant n \leqslant 13$, and back to $(CO_2)_2^-$ for $n > 13$. Fleischman and Jordan predicted,[112] based on electronic-structure calculations, that the global minimum of $(CO_2)_2^-$ corresponds to a structure of D_{2d} symmetry with the charge equally divided between the two CO_2 moieties. The $(CO_2)_2^- \rightarrow CO_2^-$ core switching in $(CO_2)_n^-$ at $n = 6$ was attributed[107,108] to a more favorable solvation of the monomer anion, compared to the covalent dimer due to the more localized charge distribution in the latter. The reverse switch occurs between $n = 13$ and 14,[108] in order to accommodate the dimer-based "magic number" structure of $(CO_2)_{14}^-$, *i.e.* $(CO_2)_2^-\cdot(CO_2)_{12}$.

Photofragmentation studies provide an alternative perspective of the structural properties and photochemistry of cluster anions. Alexander *et al.* investigated the photofragmentation of $(CO_2)_n^-$ cluster ions[136] and found that they break up exclusively to smaller species of similar composition $(CO_2)_k^-$, $k < n$. This behavior may give an impression that no bond breaking or chemical rearrangements are taking place and the fragmentation proceeds merely *via* the loss of solvent molecules. This is not necessarily the case. The ionic core of these clusters is formed by adding an electron to either the LUMO of a CO_2 monomer or to the combined LUMO of two CO_2 molecules (*i.e.*, a van der Waals dimer).[112,137] Thus, these cluster ions can be viewed as ensembles of closed-shell molecules with an access electron either localized on one of them or shared between two. The only additional covalent bond that may be formed in the cluster anion is the weak (order of 1/2) C–C bond in the D_{2d} $(CO_2)_2^-$ dimer anion predicted by Jordan and coworkers.[112] This bond is likely to be broken after absorption of a photon, and yet the resulting photofragments are described as $(CO_2)_k^-$, indistinguishable from those formed by solvent evaporation.

Given the isovalency and structural similarity of OCS and CO_2, one might expect the properties of $(OCS)_n^-$ to be similar to those of $(CO_2)_n^-$. However, the photochemistry of $(OCS)_n^-$ proved to be a striking deviation from this expectation.[113] The studies of carbonyl sulfide cluster anions began in 1998 with the Lineberger group identifying several types of ionic photofragments of $(OCS)_n^-$. In addition to $(OCS)_k^-$, which could be expected by analogy with $(CO_2)_n^-$, the observed products included S_2^- and S^-/OCS_2^- based photofragments.[113] Such variety of fragmentation channels suggested that extensive bond-breaking and chemical rearrangements take place in the cluster fragmentation process.

These observations were attributed[113] to the existence of electronic isomers of $(OCS)_n^-$.[114,115] In particular, the abundance of the S_2^--based fragments hinted at the role of a covalently bound dimer anion cluster core with S–S bonding. In collaboration with Jordan, the Lineberger group examined the properties of three $(OCS)_2^-$ isomers, whose calculated structures and relative energies are shown in Fig. 9.[113,137] All $(OCS)_n^-$ cluster ions are believed to be based on one of the core species shown in Fig. 9.

The first $(OCS)_2^-$ isomer shown in Fig. 9(a) is an electrostatically bound cluster of OCS^- with one OCS solvent molecule. The $(OCS)_n^-$ cluster ions with an OCS^- core, adapting the structural motif of Fig. 9(a), are analogous to the CO_2^- based cluster ions of $(CO_2)_n^-$, $n = 7$–13.[107,108] The covalently bound isomer of C_2 symmetry shown in Fig. 9(b) has a C–C bond of the order of 1/2 and is similar to the D_{2d} dimer structure of $(CO_2)_2^-$ predicted by Jordan and co-workers.[112] Fig. 9(c) shows a cyclic dimer anion of C_{2v} symmetry, whose likely photochemical signature is the formation of the S_2^- fragments. A species of this kind was first observed[113] in $(OCS)_n^-$, followed by the discovery of similar anions of $(CS_2)_2^-$.[106,109,138] In particular, the existence of such structures was revealed in a photodetachment study of $(CS_2)_n^-$ by Tsukuda *et al.*[109] and further confirmed by the observation of $C_2S_2^-$ products in the photodissociation of $(CS_2)_n^-$.[106] In this light, it may appear intriguing that no cyclic structures were observed in the experiments on $(CO_2)_n^-$.[107,108,136]

As described by Jordan and co-workers,[113,137,138] the

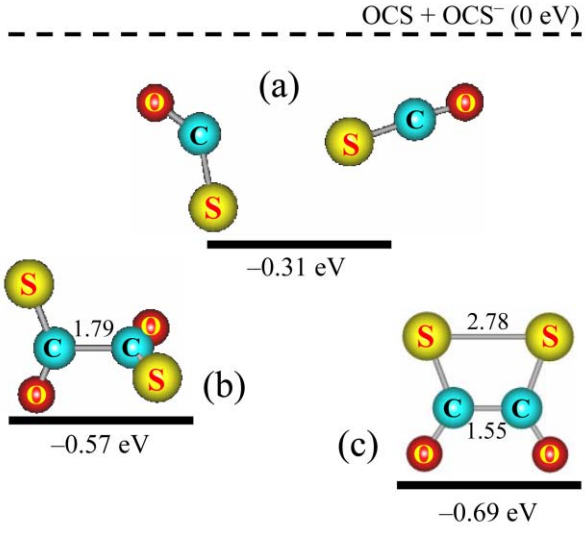

Fig. 9 Equilibrium geometries and relative energies of three $(OCS)_2^-$ species optimized at the MP2/6-31+G(d) level of theory. (a) Electrostatically bound $OCS^-\cdot OCS$ cluster anion (planar structure). (b) C_2 symmetry structure with a C–C bond of the order of 1/2. (c) C_{2v} symmetry structure corresponding to the global potential minimum of $(OCS)_2^-$ with a $^2B_2$ symmetry electronic wave function and C–C and S–S bond orders of 1 and 1/2, respectively. Some important bond lengths are indicated in ångströms. The energies given were calculated relative to the OCS + OCS^- limit and include harmonic zero-point vibration energy corrections determined at the HF/6-31+G* level). Data from ref. 113.

$(OCS)_2^-$ anion in Fig. 9(c) differs from the other covalent species shown in Fig. 9(b) in that its electronic structure is not derived directly from ground-state OCS or its van der Waals dimer. In the molecular-orbital picture, the removal of the excess electron from the $(OCS)_2^-$ anion shown in Fig. 9(b) yields two OCS molecules in the ground electronic states. To the contrary, the detachment from the HOMO of the cyclic dimer is predicted to access a metastable state of $(OCS)_2$, whose electronic configuration is doubly excited with respect to that of two ground-state OCS molecules. Its electronic configuration arises from a singlet coupling of two OCS molecules excited to the lowest triplet states. Most, but not all, of the combined singlet–triplet excitation energy for two OCS molecules is recovered by the strong bonding in the doubly excited neutral dimer, in which both the C–C and S–S bonds are of the order of 1. Adding an electron to its low-lying LUMO yields the ground ($^2B_2$) state of $(OCS)_2^-$, whose equilibrium geometry is shown in Fig. 9(c).[113,137] In similar ways, the energetics of the $(CO_2)_2^-$, $(OCS)_2^-$, and $(CS_2)_2^-$ cyclic anions are dependent, in part, on the singlet–triplet splitting in the respective neutral monomers. In CO_2, this splitting is significantly larger than in OCS or CS_2, and as a result, the cyclic dimer anion of CO_2 is less stable.[137]

The properties of $(OCS)_2^-$ raise general questions about the reactivity of negative ions in homogeneous *versus* heterogeneous cluster environments. In particular, to characterize the electronic and structural isomers, one needs to discriminate between the covalent and electrostatically bound species. Heterogeneous clusters offer opportunities to study the interactions of the anion (*e.g.*, OCS^-) with the solvent under conditions when the charge localization is known and unambiguous. A case in point is $OCS^-\cdot H_2O$. Because of the slightly negative EA of OCS, OCS^- is believed to be metastable[139] and cannot be formed efficiently in a standard ion source. In hydrated clusters, the anion is stabilized by interactions with the solvent and detailed examination of OCS^- properties is possible.

To illustrate this point, Fig. 10 displays a negative-ion mass spectrum[139] obtained using standard pulsed ion source techniques[3] with the OCS precursor seeded in Ar with trace amount of water. In comparison to other ions, almost no OCS^- is detected. On the other hand, there is an intense progression of peaks corresponding to $OCS^-(H_2O)_k$ with k ranging from 1 to at least 5. Another intense peak in the spectrum corresponds to $(OCS)_2^-$. Thus, while OCS^- is not formed efficiently by itself, it is stabilized by either electrostatic of chemical interactions.

A new approach to negative-ion photoelectron spectroscopy is based on photoelectron imaging. The imaging approach to gas-phase dynamics was originally developed by Chandler and Houston[76,140] as a tool of photofragment spectroscopy for studying the photodissociation of neutral molecules.[140,141] Several recent breakthroughs in imaging technology[142–145] led to an explosive growth in the field and made the application of imaging to negative ions very compelling. Among the recent advances in imaging are: velocity-map imaging,[142,143] which results in resolution comparable to that of other spectroscopic techniques; event counting,[144,145] which makes it possible to carry out measurements with very low signals; and the Basis Set Expansion method of Reisler and co-workers, which revolutionalized the data analysis.[146]

The application of imaging to negative-ion photoelectron spectroscopy was implemented recently by the groups of Broyer,[80,81] Continetti,[83] Neumark,[147] and Sanov.[82,115,148] The coincidence measurements of photoelectron–photofragment angular correlation and energy partitioning in dissociative photodetachment by Continetti and co-workers demonstrated the ground-breaking capability of giving insights into the molecule-fixed photoelectron angular distributions.[70,73]

Photoelectron imaging yields three-dimensional distributions of the velocity vectors in the laboratory frame, including the photoelectron speed and angular distributions.[140] The former are converted into photoelectron spectra, while the latter reflect the electronic wave function symmetry,[149–153] serving as a portal[103,154–161] for observing the dynamics from the electronic perspective.

Here we describe the application of photoelectron imaging to $OCS^-\cdot H_2O$ and $(OCS)_2^-$. The monohydrated anion of carbonyl sulfide was predicted to have a straightforward electrostatically bound structure.[139,162] The electrostatically and covalently bound isomers of the homogeneous dimer anion, *i.e.*, $OCS^-\cdot OCS$ and $(OCS)_2^-$, are discussed above. Comparison of the $OCS^-\cdot H_2O$ and $OCS^-\cdot OCS/(OCS)_2^-$ photoelectron imaging fingerprints gives insights into the electronic structure, as well as the intimate interplay between the gas-phase and bulk properties of matter.

Fig. 11 shows a series of photoelectron images of $OCS^-\cdot H_2O$ and $(OCS)_2^-$ obtained by Surber and Sanov at three different laser wavelengths.[82,115] The $OCS^-\cdot H_2O$ images feature a single electronic transition with a broad Franck–Condon envelope, as characteristic of a bent-to-linear detachment transition in the OCS^- cluster core.[82] The angular anisotropy in these images has been compared to that observed for CS_2^- and found in agreement with the expected electronic structure of the anion. A qualitative s & p model was proposed that describes the observed photoelectron angular distributions in terms of the lowest ℓ-components (in many cases, limited to the s and p partial waves) of the free (photodetached) electron.[82,148]

A comparison of the $OCS^-\cdot H_2O$ and $(OCS)_2^-$ images in

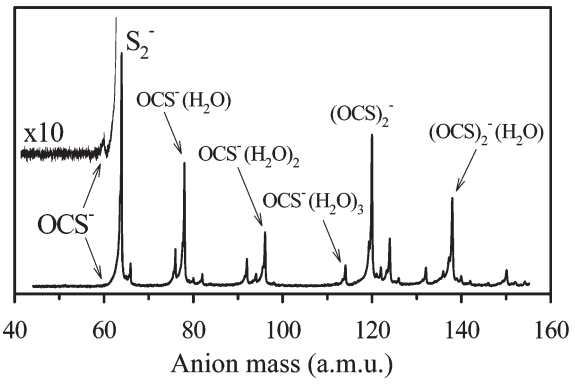

Fig. 10 Negative-ion mass-spectrum obtained with the OCS/Ar precursor with a trace of water. The magnified ($\times 10$) spectrum corresponds to experimental conditions optimized for the formation of OCS^- and shows the best OCS^- signal that could be achieved in the experiment. Adapted from ref. 139.

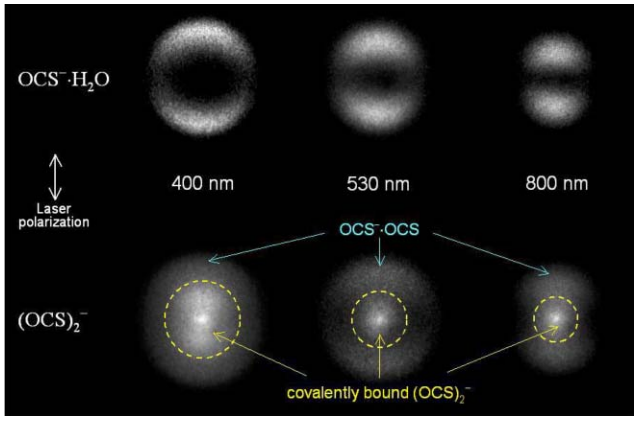

Fig. 11 Photoelectron images of $OCS^-\cdot H_2O$ (top) and $(OCS)_2^-$ (bottom) recorded at 400, 530, and 800 nm, shown on arbitrary velocity and intensity scales. The $(OCS)_2^-$ signal inside the dashed circles is attributed mainly to covalent $(OCS)_2^-$ isomers. The signal outside the dashed circles is attributed to the $OCS^-\cdot OCS$ cluster anion (electrostatically bound). Data from ref. 115.

Fig. 11 clearly reveals signatures of different $(OCS)_2^-$ isomers.[82,148] The diffuse lobes at large radii, polarized in the direction of the laser polarization (vertical in the plane of the figure), are attributed to the electrostatically bound $OCS^-\cdot OCS$ cluster anion, based on the similarity of these parts of the images to $OCS^-\cdot H_2O$. The photoelectron signatures of $OCS^-\cdot H_2O$ and $OCS^-\cdot OCS$ are expected to be similar, because in both cases the electron is ejected from a cluster molecular orbital with primarily the OCS^- HOMO character. The signal inside the dashed circles marked over the $(OCS)_2^-$ images is attributed to the covalently bound structures of the dimer anion.[115]

The OCS^-OCS and covalent $(OCS)_2^-$ anions behave differently in photoexcitation. The former species absorb light *via* direct photodetachment, resulting in the photoelectron imaging signatures described above. The covalent dimer anion, on the other hand, was predicted to possess a number of low-lying excited anionic states;[113,137,138] therefore, it can be either photodetached directly or promoted to an excited state. The excited-state decay, in turn, involves the competition between the autodetachment and fragmentation.[114,115]

In Fig. 11, the direct photodetachment of covalent $(OCS)_2^-$ is manifest as the diffuse anisotropic feature just inside the dashed circle marked over the 400 nm image. The 530 and 800 nm photon energies are not sufficient to access this transition. The autodetachment, yielding characteristically slow electrons, is seen as the intense isotropic spots at the centers of all three $(OCS)_2^-$ photoelectron images. The autodetachment spots originate from either the excited state of $(OCS)_2^-$ or the internally excited anionic photofragmentation products (*e.g.*, OCS^-). In either case, the autodetachment can be modeled[115] as a gas-phase analog of thermionic emission,[80] an effect usually associated with bulk materials. Thus, the bulk statistical model assuming strong electronic-vibrational couplings and a highly mixed nature of the excited anionic state, was found applicable to such a small system as $(OCS)_2^-$, which appears to combine both molecular and "bulk" properties.[115]

The case of $(OCS)_2^-$, as well as that of larger $(OCS)_n^-$ cluster anions,[114] is just one example that demonstrates that the answer to the question posed at the beginning of this Perspective ("How much matter is needed for physical laws associated with bulk materials to be applicable?") is: It is not the size of the microscopic object that determines the applicability of the bulk description, but the details of the electronic structure, including the availability of low-lying, mixed excited states.

The one-photon, or 'static', photoelectron images, as those shown in Fig. 11, provide insights into the electronic structure of cluster anions. A natural extension of this approach is probing the evolution of the electronic structure in photo-induced chemical reactions using femtosecond pump–probe photoelectron imaging spectroscopy. The power of this approach has been successfully demonstrated for neutral molecules by the groups of Hayden, Continetti, and Suzuki.[77,78,163–165] Femtosecond imaging experiments on molecular and cluster anions are now underway in the Neumark group at Berkeley and the Sanov group at the University of Arizona. As with traditional femtosecond photoelectron spectroscopy, the applicability of femtosecond photoelectron imaging is not limited to clusters. However, the imaging approach is particularly promising in the cluster case, as it allows examining the transformations of electronic wave functions under the effects of microscopic solvation. Cluster anions also provide unique opportunities for detailed gas-phase studies of bimolecular encounters, which can be viewed, using photoelectron and fragment imaging, from both the electronic and nuclear perspectives.

5. Summary

This Perspective reflected on several recent advances in the studies of cluster anion structure and dynamics. We discussed the effects of the solvent on the electronic structure and reactivity of negative ions in homogeneous and heterogeneous solvation environments. Some recent breakthroughs in experimental methodology were outlined, in particular the application of photofragment and photoelectron methods and the imaging technique to the studies of molecular cluster anions.

In the future, we should expect to see an increased emphasis on ultrafast coincidence dynamics in the studies of cluster ion reactivity. As more sophisticated experimental tools become available, physical chemists will be able to describe the reaction dynamics in more detailed and less averaged ways. The trend towards better-resolved and less averaged observables is seen in many recent developments, including the growing popularity of the imaging technique (complementary energy and angular distributions), a variety of coincidence methods (correlated product distributions), and time-domain measurements.

Another trend that should not be overlooked by experimentalists is the developments in theoretical chemistry, in particular the explosive growth in the computational capabilities. As demonstrated by several examples in this Perspective, the interpretation of experimental results is often dependent on extensive theoretical work. As the theoretical and experimental capabilities reach new levels of elegance and sophistication, chemists acquire the ability to tackle more intriguing questions of structure and dynamics. Many *ab initio* problems that a decade ago would have required the computing power of a supercomputer today can be solved at minimal expense using a personal machine in one's office. Thanks to this development, experimentalists can now routinely use the power of computational chemistry to obtain the initial interpretation of results enabling them to navigate more efficiently in search of scientific answers. Such skillful navigation becomes increasingly important, as the sheer dimensionality of information provided by modern state-of-the-art experiments makes their success more dependent than ever on one's ability to ask the right questions.

Acknowledgements

We thank Prof. Robert Parson and Prof. Kenneth D. Jordan for their collaborations and insights into several projects discussed in this Perspective. A. Sanov acknowledges support from the National Science Foundation grants Nos. CHE-9982057 and CHE-0134631, the Beckman Young Investigator Award, the Research Corporation Research Innovation Award No. RI0515, and the ACS PRF grant No. 35589-G6. W. C. Lineberger is pleased to acknowledge support from the National Science Foundation grants Nos. CHE-0201848 and PHY-0096822 and the Air Force Office of Scientific Research grant No. F49620-02-1-0371.

References

1 A. W. Castleman and K. H. Bowen, *J. Phys. Chem.*, 1996, **100**, 12911. ★ *An extensive review of the field of cluster research highlighting the significant advances made during the later part of the twentieth century. Published in the Centennial Issue of J. Phys. Chem.*

2 J. M. Farrar, in *Current Topics in Ion Chemistry and Physics*, ed. C. Y. Ng and I. Powis, Wiley, New York, 1992.

3 M. A. Johnson and W. C. Lineberger, in *Techniques for the Study of Ion Molecule Reactions*, ed. J. M. Farrar and J. W. Saunders, Wiley, New York, 1988, p. 591. ★ *The original review of the pulsed methods of cluster ion spectroscopy extensively used by many research groups in the negative-ion community throughout the world.*

4 A. W. Castleman, Jr., in *Clusters of Atoms and Molecules*, ed. H. Haberland, Springer-Verlag, New York, 1992.

5 J. C. Alfano, Y. Kimura, P. K. Walhout and P. F. Barbara, *Chem. Phys. Chem.*, 1993, **175**, 143. ★ *Experimental study of I_2^- photodissociation and vibrational relaxation in water and ethanol.*

6 D. A. V. Kliner, J. C. Alfano and P. F. Barbara, *J. Chem. Phys.*, 1993, **98**, 5375.

7 P. K. Walhout, J. C. Alfano, K. A. M. Thakur and P. F. Barbara, *J. Phys. Chem.*, 1995, **99**, 7568.
8 U. Banin and S. Ruhman, *J. Chem. Phys.*, 1993, **98**, 4391.
9 E. Gershgoren, U. Banin and S. Ruhman, *J. Phys. Chem. A*, 1998, **102**, 9.
10 H. Yasumatsu, S. Koizumi, A. Terasaki and T. Kondow, *J. Chem. Phys.*, 1996, **105**, 9509.
11 H. Yasumatsu, A. Terasaki and T. Kondow, *J. Chem. Phys.*, 1997, **106**, 3806.
12 F. G. Amar and L. Perera, *Z. Phys. D*, 1991, **20**, 173.
13 B. J. Gertner, K. Ando, R. Bianco and J. T. Hynes, *Chem. Phys.*, 1994, **183**, 309.
14 R. Bianco and J. T. Hynes, *J. Chem. Phys.*, 1995, **102**, 7864.
15 R. Bianco and J. T. Hynes, *J. Chem. Phys.*, 1995, **102**, 7885.
16 I. Benjamin, P. F. Barbara, B. J. Gertner and J. T. Hynes, *J. Phys. Chem.*, 1995, **99**, 7557.
17 B. J. Greenblatt, M. T. Zanni and D. M. Neumark, *Chem. Phys. Lett.*, 1996, **258**, 523.
18 M. T. Zanni, T. R. Taylor, B. J. Greenblatt, B. Soep and D. M. Neumark, *J. Chem. Phys.*, 1997, **107**, 7613.
19 M. T. Zanni, V. S. Batista, B. J. Greenblatt, W. H. Miller and D. M. Neumark, *J. Chem. Phys.*, 1999, **110**, 3748.
20 D. Ray, N. E. Levinger, J. M. Papanikolas and W. C. Lineberger, *J. Chem. Phys.*, 1989, **91**, 6533.
21 J. M. Papanikolas, V. Vorsa, M. E. Nadal, P. J. Campagnola, H. K. Buchenau and W. C. Lineberger, *J. Chem. Phys.*, 1993, **99**, 8733. ★ *Experimental study of I_2^- photodissociation and recombination dynamics in size-selected CO_2 clusters.*
22 S. Nandi, A. Sanov, N. Delaney, J. Faeder, R. Parson and W. C. Lineberger, *J. Phys. Chem. A*, 1998, **102**, 8827. ★ *The first report of I_2^- caging in clusters of OCS involving fast spin–orbit relaxation.*
23 A. Sanov, S. Nandi and W. C. Lineberger, *J. Chem. Phys.*, 1998, **108**, 5155.
24 A. Sanov, T. Sanford, S. Nandi and W. C. Lineberger, *J. Chem. Phys.*, 1999, **111**, 664. ★ *Time-resolved study of photofragment caging involving fast quenching of spin–orbit excited iodine by solvent-asymmetry mediated electron transfer.*
25 J. M. Papanikolas, J. R. Gord, N. E. Levinger, D. Ray, V. Vorsa and W. C. Lineberger, *J. Phys. Chem.*, 1991, **95**, 8028.
26 J. Troe, *Annu. Rev. Phys. Chem.*, 1978, **29**, 223.
27 B. Otto, J. Schroeder and J. Troe, *J. Chem. Phys.*, 1984, **81**, 202.
28 H. Kunz, J. G. McCaffrey, R. Schriever and N. Schwentner, *J. Chem. Phys.*, 1991, **94**, 1039.
29 J. Xu, N. Schwentner and M. Chergui, *J. Chem. Phys.*, 1994, **101**, 7381.
30 K. H. Godderz, N. Schwentner and M. Chergui, *J. Chem. Phys.*, 1996, **105**, 451.
31 V. E. Bondybey and L. E. Brus, *Adv. Chem. Phys.*, 1980, **41**, 269.
32 P. S. Dardi and J. S. Dahler, *J. Chem. Phys.*, 1990, **93**, 242.
33 G. N. R. Tripathi, R. H. Schuler and R. W. Fessenden, *Chem. Phys. Lett.*, 1985, **113**, 563.
34 V. S. Batista and D. F. Coker, *J. Chem. Phys.*, 1997, **106**, 7102.
35 B. M. Ladanyi and R. Parson, *J. Chem. Phys.*, 1997, **107**, 9326.
36 N. Delaney, J. Faeder, P. E. Maslen and R. Parson, *J. Phys. Chem. A*, 1997, **101**, 8147.
37 X. Xu, S. Yu, R. Lingle, H. Zhu and J. B. Hopkins, *J. Chem. Phys.*, 1991, **95**, 2445.
38 A. L. Harris, J. K. Brown and C. B. Harris, *Annu. Rev. Phys. Chem.*, 1988, **39**, 341.
39 R. Zadoyan, Z. Li, C. C. Martens and V. A. Apkarian, *J. Chem. Phys.*, 1994, **101**, 6648.
40 R. Zadoyan, Z. Li, P. Ashjian, C. C. Martens and V. A. Apkarian, *Chem. Phys. Lett.*, 1994, **218**, 504.
41 Q. Liu, J. K. Wang and A. H. Zewail, *Nature*, 1993, **364**, 427.
42 E. D. Potter, Q. Liu and A. H. Zewail, *Chem. Phys. Lett.*, 1992, **200**, 605.
43 Q. L. Liu, J. K. Wang and A. H. Zewail, *J. Phys. Chem.*, 1995, **99**, 11321.
44 J. K. Wang, Q. L. Liu and A. H. Zewail, *J. Phys. Chem.*, 1995, **99**, 11309.
45 A. E. Johnson, N. E. Levinger and P. F. Barbara, *J. Phys. Chem.*, 1992, **96**, 7841.
46 B. J. Greenblatt, M. T. Zanni and D. M. Neumark, *Science*, 1997, **276**, 1675. ★ *A landmark study of dynamics of $I_2^-Ar_6$ and $I_2^-Ar_{20}$ subsequent to photodissociation of the I_2^- chromophore using femtosecond photoelectron spectroscopy.*
47 R. Parson and J. Faeder, *Science*, 1997, **276**, 1660. ★ *A theoretical perspective on the Neumark group's study of $I_2^-Ar_n$ dynamics by femtosecond PES.*
48 J. M. Papanikolas, V. Vorsa, M. E. Nadal, P. J. Campagnola, J. R. Gord and W. C. Lineberger, *J. Chem. Phys.*, 1992, **97**, 7002.
49 V. Vorsa, S. Nandi, P. J. Campagnola, M. Larsson and W. C. Lineberger, *J. Chem. Phys.*, 1997, **106**, 1402. ★ *Time-resolved study of photodissociation and recombination dynamics of I_2^- in size-selected Ar and CO_2 clusters.*
50 V. Vorsa, P. J. Campagnola, S. Nandi, M. Larsson and W. C. Lineberger, *J. Chem. Phys.*, 1996, **105**, 2298. ★ *Observation of metastable solvent-separated $(I\text{–}\cdots I)\ Ar_m$ photofragments, where the I_2^- bond has not reformed.*
51 J. M. Papanikolas, P. J. Campagnola, V. Vorsa, M. E. Nadal, H. K. Buchenau, R. Parson and W. C. Lineberger, in *The Chemical Dynamics and Kinetics of Small Radicals*, ed. K. Liu and A. Wagner, World Scientific Publishing Co., Singapore, 1995, vol. 6, p. 616.
52 M. E. Nadal, P. D. Kleiber and W. C. Lineberger, *J. Chem. Phys.*, 1996, **105**, 504.
53 A. Sanov and W. C. Lineberger, *Proc. SPIE*, 1998, **3271**, 188.
54 E. Rabinowitch and W. C. Wood, *Trans. Faraday Soc.*, 1936, **32**, 547.
55 E. Rabinowitch and W. C. Wood, *Trans. Faraday Soc.*, 1936, **32**, 1381.
56 J. Franck and E. Rabinowitch, *Trans. Faraday Soc.*, 1934, **30**, 120.
57 J. Xu, N. Schwentner, S. Hennig and M. Chergui, *J. Chim. Phys. Phys. Chim Biol.*, 1995, **92**, 541.
58 Z. Li, R. Zadoyan, V. A. Apkarian and C. C. Martens, *J. Phys. Chem.*, 1995, **99**, 7453.
59 V. S. Batista and D. F. Coker, *J. Chem. Phys.*, 1997, **106**, 6923.
60 P. E. Maslen, J. M. Papanikolas, J. Faeder, R. Parson and S. V. ONeil, *J. Chem. Phys.*, 1994, **101**, 5731.
61 P. E. Maslen, J. Faeder and R. Parson, *Chem. Phys. Lett.*, 1996, **263**, 63. ★ *Ab initio study of I_2^- electronic states.*
62 J. Faeder, N. Delaney, P. E. Maslen and R. Parson, *Chem. Phys.*, 1998, **239**, 525.
63 N. Delaney, J. Faeder and R. Parson, *J. Chem. Phys.*, 1999, **111**, 651. ★ *Presentation of the solvent-asymmetry mediated electron transfer model of spin–orbit quenching involved in the near-UV caging of I_2^-.*
64 J. H. D. Eland, *Photoelectron Spectroscopy*, Butterworths, London, 1984. ★ *A classic book on photoelectron spectroscopy.*
65 K. M. Ervin and W. C. Lineberger, in *Advances in Gas Phase Ion Chemistry*, ed. N. G. Adams and L. M. Babcock, JAI Press, Greenwich, 1992, vol. 1, p. 121. ★ *A review of photoelectron spectroscopy of negative ions.*
66 W. C. Lineberger, M. E. Nadal, P. J. Campagnola, V. Vorsa, P. D. Kleiber, J. M. Papanikolas, P. E. Maslen, J. Faeder, R. Parson and O. Poplawski, in *Proceedings of The Robert A. Welch Foundation 38th Conference on Chemical Research: Chemical Dynamics of Transient Species*, R. A. Welch Foundation, Houston, TX, 1994, vol. 38, p. 175.
67 J. H. D. Eland, *Mol. Phys.*, 1987, **61**, 725.
68 J. H. D. Eland, *J. Electron Spectrosc. Relat. Phenom.*, 2000, **112**, 1. ★ *A presentation of novel coincidence techniques for the study of single photon double ionization.*
69 K. A. Hanold, C. R. Sherwood and R. E. Continetti, *J. Chem. Phys.*, 1995, **103**, 9876. ★ *A landmark study of photoelectron–neutral–neutral coincidence dynamics of dissociative photodetachment of O_4^-.*
70 K. A. Hanold, M. C. Garner and R. E. Continetti, *Phys. Rev. Lett.*, 1996, **77**, 3335. ★ *A beautiful coincidence measurement of photoelectron–photofragment angular correlation and energy partitioning in the dissociative photodetachment of O_4^- providing insights into the molecule-fixed photoelectron angular distribution of a negative ion.*
71 T. Baer and Y. Li, *Int. J. Mass Spectrom.*, 2002, **219**, 381.
72 T. Baer, *Int. J. Mass Spectrom.*, 2000, **200**, 443. ★ *Review of photoelectron–photoion coincidence (PEPICO) spectroscopy.*
73 R. E. Continetti, *Annu. Rev. Phys. Chem.*, 2001, **52**, 165. ★ *An extensive review of coincidence techniques in the studies of the reaction dynamics of isolated molecules.*
74 P. Ayotte, G. H. Weddle, C. G. Bailey, M. A. Johnson, F. Vila and K. D. Jordan, *J. Chem. Phys.*, 1999, **110**, 6268. ★ *A benchmark study of negatively charged water clusters by infrared spectroscopy.*
75 C. G. Bailey, J. Kim and M. A. Johnson, *J. Phys. Chem.*, 1996, **100**, 16782.
76 D. W. Chandler and P. L. Houston, *J. Chem. Phys.*, 1987, **87**, 1445. ★ *This pioneering paper describes the original photofragment ion imaging experiment. The entire field of photofragment and photoelectron imaging developed from this work.*

77 J. A. Davies, J. E. LeClaire, R. E. Continetti and C. C. Hayden, *J. Chem. Phys.*, 1999, **111**, 1. ★ *A pioneering application of femtosecond time-resolved photoelectron–photoion coincidence imaging to studies of neutral dissociation dynamics.*
78 L. Wang, H. Kohguchi and T. Suzuki, *Faraday Discuss.*, 1999, **113**, 37. ★ *The first demonstration of femtosecond photoelectron imaging used to probe dynamics in neutral molecules.*
79 C. Bordas, J. C. Pinare, B. Baguenard and M. Broyer, *J. Phys. IV*, 2000, **10**, 55.
80 B. Baguenard, J. C. Pinare, C. Bordas and M. Broyer, *Phys. Rev. A*, 2001, **63**, art. no. 023204. ★ *Photoelectron imaging study of tungsten cluster anions.*
81 B. Baguenard, J. C. Pinare, F. Lepine, C. Bordas and M. Broyer, *Chem. Phys. Lett.*, 2002, **352**, 147. ★ *Photoelectron imaging study of carbon cluster anions.*
82 E. Surber and A. Sanov, *J. Chem. Phys.*, 2002, **116**, 5921.
83 H. J. Deyerl, L. S. Alconcel and R. E. Continetti, *J. Phys. Chem. A*, 2001, **105**, 552.
84 J. M. Papanikolas, P. E. Maslen and R. Parson, *J. Chem. Phys.*, 1995, **102**, 2452.
85 J. Faeder, PhD Thesis, University of Colorado, 1998.
86 M. R. Battaglia, A. D. Buckingham, D. Neumark, R. K. Pierens and J. H. Williams, *Mol. Phys.*, 1981, **43**, 1015.
87 A. D. Buckingham, C. Graham and J. H. Williams, *Mol. Phys.*, 1988, **49**, 703.
88 J. Faeder, N. Delaney, P. E. Maslen and R. Parson, *Chem. Phys. Lett.*, 1997, **270**, 196.
89 M. E. Nadal, PhD Thesis, University of Colorado, 1996.
90 H. Yasumatsu, U. Kalmbach, S. Koizumi, A. Terasaki and T. Kondow, *Z. Phys. D*, 1997, **40**, 1.
91 H. Yasumatsu, T. Tsukuda, T. Sugai, A. Terasaki, T. Nagata and T. Kondow, *Surf. Rev. Lett.*, 1996, **3**, 901.
92 N. Delaney, J. Faeder and R. Parson, *J. Chem. Phys.*, 1999, **111**, 452.
93 J. Faeder and R. Parson, *J. Chem. Phys.*, 1998, **108**, 3909.
94 B. J. Greenblatt, M. T. Zanni and D. M. Neumark, *J. Chem. Phys.*, 2000, **112**, 601.
95 A. V. Davis, R. Wester, A. E. Bragg and D. M. Neumark, *J. Chem. Phys.*, 2002, **117**, 4282.
96 R. Wester, A. V. Davis, A. E. Bragg and D. M. Neumark, *Phys. Rev. A*, 2002, **65**, art. no. 051201.
97 B. J. Greenblatt, M. T. Zanni and D. M. Neumark, *J. Chem. Phys.*, 1999, **111**, 10566.
98 D. Husain and R. J. Donovan, in *Advances in Photochemistry*, ed. J. N. Pitts, Jr., G. S. Hammond, and W. A. Noyers, Jr., Wiley-Interscience, New York–London–Sydney–Toronto, vol. 8, 1971.
99 A. H. Zewail, in *Chemical Reactions and Their Control on the Femto-second Time Scale: XXth Solvay Conference On Chemistry*, John Wiley & Sons Inc, New York, 1997, vol. 101, p. 892.
100 A. H. Zewail, *J. Phys. Chem. A*, 2000, **104**, 5660. ★ *An anthology adapted from the Nobel Lecture, which gives an overview of the field of femtochemistry from the author's perspective.*
101 A. H. Zewail, *Pure Appl. Chem.*, 2000, **72**, 2219. ★ *A historical perspective of the development of femtochemistry.*
102 J. S. Baskin and A. H. Zewail, *J. Chem. Educ.*, 2001, **78**, 737.
103 S. Lochbrunner, J. J. Larsen, J. P. Shaffer, M. Schmitt, T. Schultz, J. G. Underwood and A. Stolow, *J. Electron Spectrosc. Relat. Phenom.*, 2000, **112**, 183. ★ *A detailed discussion of femtosecond time-resolved photoelectron spectroscopy as a technique for investigating excited state dynamics.*
104 V. Blanchet, M. Z. Zgierski, T. Seideman and A. Stolow, *Nature*, 1999, **401**, 52. ★ *A popular description of applications of time-resolved photoelectron spectroscopy to discerning vibronic molecular dynamics.*
105 G. Gantefor, S. Kraus and W. Eberhardt, *J. Electron Spectrosc. Relat. Phenom.*, 1998, **88**, 35.
106 T. Maeyama, T. Oikawa, T. Tsumura and N. Mikami, *J. Chem. Phys.*, 1998, **108**, 1368.
107 M. J. DeLuca, B. Niu and M. A. Johnson, *J. Chem. Phys.*, 1988, **88**, 5857. ★ *The original demonstration of core-switching in $(CO_2)_n^-$ cluster anions.*
108 T. Tsukuda, M. A. Johnson and T. Nagata, *Chem. Phys. Lett.*, 1997, **268**, 429.
109 T. Tsukuda, T. Hirose and T. Nagata, *Chem. Phys. Lett.*, 1997, **279**, 179.
110 K. H. Bowen and J. G. Eaton, in *The Structure of Small Molecules and Ions*, ed. R. Naaman and Z. Vager, Plenum, New York, 1988, p. 147.
111 K. Hiraoka, S. Fujimaki, G. Aruga and S. Yamabe, *J. Phys. Chem.*, 1994, **98**, 1802.
112 S. H. Fleischman and K. D. Jordan, *J. Phys. Chem.*, 1987, **91**, 1300. ★ *The first theoretical prediction of the covalently bound dimer anion of CO_2.*
113 A. Sanov, S. Nandi, K. D. Jordan and W. C. Lineberger, *J. Chem. Phys.*, 1998, **109**, 1264. ★ *The original experimental study of $(OCS)_n^-$ photochemistry.*
114 E. Surber, R. Mabbs and A. Sanov, in preparation. ★ *This paper describes photoelectron imaging experiments on carbonyl sulfide cluster anions, focusing on the isomer coexistence and competition of excited-state decay mechanisms.*
115 E. Surber and A. Sanov, *Phys. Rev. Lett.*, submitted. ★ *This letter addresses imaging of direct photodetachment and delayed autodetachment of $(OCS)_2^-$, emphasizing the excited-state dynamics of the covalent dimer anion.*
116 J. Jortner, M. Ottolenghi and G. Stein, *J. Phys. Chem.*, 1964, **68**, 247.
117 P. Ayotte and M. A. Johnson, *J. Chem. Phys.*, 1997, **106**, 811.
118 D. W. Arnold, S. E. Bradforth, E. H. Kim and D. M. Neumark, *J. Chem. Phys.*, 1992, **97**, 9468.
119 Y. X. Zhao, C. C. Arnold and D. M. Neumark, *J. Chem. Soc., Faraday Trans.*, 1993, **89**, 1449.
120 A. Sanov, J. Faeder, R. Parson and W. C. Lineberger, *Chem. Phys. Lett.*, 1999, **313**, 812.
121 C. G. Bailey, J. Kim, C. E. H. Dessent and M. A. Johnson, *Chem. Phys. Lett.*, 1997, **269**, 122.
122 P. Ayotte, G. H. Weddle, J. Kim and M. A. Johnson, *Chem. Phys.*, 1998, **239**, 485.
123 P. Ayotte, G. H. Weddle and M. A. Johnson, *J. Chem. Phys.*, 1999, **110**, 7129.
124 P. Ayotte, S. B. Nielsen, G. H. Weddle, M. A. Johnson and S. S. Xantheas, *J. Phys. Chem. A*, 1999, **103**, 10665.
125 S. A. Corcelli, J. A. Kelley, J. C. Tully and M. A. Johnson, *J. Phys. Chem. A*, 2002, **106**, 4872.
126 E. A. Woronowicz, W. H. Robertson, G. H. Weddle, M. A. Johnson, E. M. Myshakin and K. D. Jordan, *J. Phys. Chem. A*, 2002, **106**, 7086.
127 S. E. Bradforth and P. Jungwirth, *J. Phys. Chem. A*, 2002, **106**, 1286.
128 I. Becker, G. Markovich and O. Cheshnovsky, *Phys. Rev. Lett.*, 1997, **79**, 3391.
129 I. Becker and O. Cheshnovsky, *J. Chem. Phys.*, 1999, **110**, 6288.
130 L. Lehr, M. T. Zanni, C. Frischkorn, R. Weinkauf and D. M. Neumark, *Science*, 1999, **284**, 635.
131 M. T. Zanni, C. Frischkorn, A. V. Davis and D. M. Neumark, *J. Phys. Chem. A*, 2000, **104**, 2527.
132 A. V. Davis, M. T. Zanni, C. Frischkorn and D. M. Neumark, *Abstr. Pap. Am. Chem. Soc.*, 1999, **218**, 186.
133 C. Frischkorn, M. T. Zanni, A. V. Davis and D. M. Neumark, *Faraday Discuss.*, 2000, 49.
134 J. Kim, I. Becker, O. Cheshnovsky and M. A. Johnson, *Chem. Phys. Lett.*, 1998, **297**, 90.
135 G. H. Lee, S. T. Arnold, J. G. Eaton, H. W. Sarkas, K. H. Bowen, C. Ludewigt and H. Haberland, *Z. Phys. D: At., Mol. Clusters*, 1991, **20**, 9.
136 M. L. Alexander, M. A. Johnson, N. E. Levinger and W. C. Lineberger, *Phys. Rev. Lett.*, 1986, **57**, 976.
137 A. Sanov, W. C. Lineberger and K. D. Jordan, unpublished.
138 A. Sanov, W. C. Lineberger and K. D. Jordan, *J. Phys. Chem. A*, 1998, **102**, 2509.
139 E. Surber, S. P. Ananthavel and A. Sanov, *J. Chem. Phys.*, 2002, **116**, 1920.
140 A. J. R. Heck and D. W. Chandler, *Annu. Rev. Phys. Chem.*, 1995, **46**, 335. ★ *A classic review of the photofragment ion imaging technique.*
141 P. L. Houston, *Acc. Chem. Res.*, 1995, **28**, 453. ★ *An excellent tutorial review of applications of imaging to studies of chemical reaction dynamics.*
142 A. T. J. B. Eppink and D. H. Parker, *Rev. Sci. Instrum.*, 1997, **68**, 3477. ★ *The pioneering introduction of velocity-map imaging. This paper revolutionized the applications of imaging to chemical dynamics.*
143 D. H. Parker and A. T. J. B. Eppink, *J. Chem. Phys.*, 1997, **107**, 2357.
144 L. J. Rogers, M. N. R. Ashfold, Y. Matsumi, M. Kawasaki and B. J. Whitaker, *Chem. Phys. Lett.*, 1996, **258**, 159.
145 B. Y. Chang, R. C. Hoetzlein, J. A. Mueller, J. D. Geiser and P. L. Houston, *Rev. Sci. Instrum.*, 1998, **69**, 1665.
146 V. Dribinski, A. Ossadtchi, V. A. Mandelshtam and H. Reisler, *Rev. Sci. Instrum.*, 2002, **73**, 2634. ★ *Introduction of the Gaussian BAsis-Set EXpansion (BASEX) approach to Abel transformation used in image analysis.*
147 D. M. Neumark, *Abstr. Pap. Am. Chem. Soc.*, 2002, **223**, 137.

148 E. Surber, R. Mabbs and A. Sanov, in preparation.
149 J. Cooper and R. N. Zare, *J. Chem. Phys.*, 1968, **49**, 4252.
150 J. Cooper and R. N. Zare, *J. Chem. Phys.*, 1968, **48**, 942.
151 J. Cooper and R. N. Zare, in *Atomic Collision Processes*, ed. S. Geltman, K. T. Mahanthappa, and W. E. Brittin, Gordon and Breach, Science Publishers, New York–London–Paris, 1968, vol. XI-C, p. 317.
152 S. Geltman, *Phys. Rev.*, 1958, **112**, 176.
153 K. J. Reed, A. H. Zimmerman, H. C. Andersen and J. I. Brauman, *J. Chem. Phys.*, 1976, **64**, 1368.
154 T. Seideman, *J. Chem. Phys.*, 1997, **107**, 7859.
155 T. Seideman, *J. Chem. Phys.*, 2000, **113**, 1677.
156 T. Seideman, *Phys. Rev. A*, 2001, **6404**, art. no. 042504.
157 T. Seideman, *Annu. Rev. Phys. Chem.*, 2002, **53**, 41. ★ *A detailed review of the utility of photoelectron angular distributions as probes of molecular dynamics*.
158 V. Blanchet, S. Lochbrunner, M. Schmitt, J. P. Shaffer, J. J. Larsen, M. Z. Zgierski, T. Seideman and A. Stolow, *Faraday Discuss.*, 2000, **115**, 33.
159 V. Blanchet, M. Z. Zgierski and A. Stolow, *J. Chem. Phys.*, 2001, **114**, 1194.
160 M. Schmitt, S. Lochbrunner, J. P. Shaffer, J. J. Larsen, M. Z. Zgierski and A. Stolow, *J. Chem. Phys.*, 2001, **114**, 1206.
161 S. Lochbrunner, T. Schultz, M. Schmitt, J. P. Shaffer, M. Z. Zgierski and A. Stolow, *J. Chem. Phys.*, 2001, **114**, 2519.
162 M. A. Johnson, personal communication.
163 J. A. Davies, R. E. Continetti, D. W. Chandler and C. C. Hayden, *Phys. Rev. Lett.*, 2000, **84**, 5983.
164 T. Suzuki, L. Wang and H. Kohguchi, *J. Chem. Phys.*, 1999, **111**, 4859.
165 M. Tsubouchi, B. J. Whitaker, L. Wang, H. Kohguchi and T. Suzuki, *Phys. Rev. Lett.*, 2001, **86**, 4500.